Earthquakes and Structures, *Vol. 10, No. 5 (2016) 1111-1123*
DOI: http://dx.doi.org/10.12989/eas.2016.10.5.1111

Experimental study on seismic performances of steel frame-bent structures

Jiongfeng Liang*[1,2], Lian S.Gu[1] and Ming H. Hu[1]

[1]Faculty of Civil & Architecture Engineering, East China Institute of Technology, Nanchang 330013, China
[2]Guangxi Key Laboratory of Disaster Prevention and Structural Safety, Guangxi University, Nanning 530004, China

(Received July 23, 2015, Revised October 16, 2015, Accepted February 29, 2016)

Abstract. To study seismic performance of steel frame-bent structure, one specimen with one-tenth scale, three-bay, and five-story was tested under reversed cyclic lateral load. The entire loading process and failure mode were observed, and the seismic performance indexes including hysteretic loops, skeleton curve, ductility, load bearing capacity, drift ratio, energy dissipation capacity and stiffness degradation were analyzed. The results show that the steel frame-bent structure has good seismic performance. And the ductility and the energy dissipation capacity were good, the hysteresis loops were in spindle shape, which shape were full and had larger area. The ultimate elastic-plastic drift ratio is larger than the limit value specified by seismic code, showing the high capacity of collapse resistance. It can be helpful to design this kind of structure in high-risk seismic zone.

Keywords: steel; frame-bent structure; cyclic lateral load; seismic performance; ductility

1. Introduction

In the steel structural system, steel frame-bent structures became a primary lateral load resisting systems in the power plant main building. Steel frame-bent consists of multistory frame and single-story bent frame system. By far, the seismic behavior and seismic design of steel frames has been investigated by a number of researchers.

Banihashemi *et al*. (2015) presented the development of performance based plastic design (PBPD) method for steel moment frames with considering the gravity loads and P-Δ effects. Stamatopoulos (2014) examined the influence of the steel column base plate semi-rigid behaviour on the seismic behaviour of steel frames. Kamaris *et al*. (2015) developed a new method for seismic design of plane steel moment resisting framed structures. Grande and Rasulo (2015) proposed a simple approach for seismic retrofit of low-rise concentric X-braced steel frames. Hsu and Li (2015) found that the strength and energy dissipation capacity of the knee braced moment resisting frame was significantly enhanced regardless of whether the knee braces buckled in the in-place or out-of-plane direction and suggested that br-aces with in- plane frame structure designs.

Pollino (2015) evaluated the dynamic response of buckling modes be adopted for greater

*Corresponding author, Ph.D., E-mail: jiongfeng108@126.com

http://www.techno-press.com/journals/eas&subpage=7 ISSN: 2092-7614 (Print), 2092-7622 (Online)

earthquake resistance in knee braced moment resisting rocking steel braced frames, such as inter-story drift and floor acceleration evaluation, etc. Nguyen and Kim (2014) presented a simple, effective numerical procedure based on the beam-column method by using the based-displacement finite element method for nonlinear inelastic time-history analysis of three-dimensional semi-rigid steel frames. Tenchini *et al.* (2014) analysed the overall seismic performance of dual-steel moment resisting frames through static and dynamic nonlinear analysis method. The results showed that the use of high strength steel in Eurocode 8 compliant mild carbon steel was effective to provide overall ductile mechanism, but it may lead to inefficient and uneconomical structures characterized by limited plastic demand due to the large design over-strength. Grande and Rasulo (2013) proposed a simplified approach for the assessment of steel braced frames with X configuration according to a procedure developed in the light of the Direct Displacement Based Design method (DDBD). Metelli (2013) designed a reduced scale test bench to study X braced steel frames with different geometrical characteristics of diagonal members and with restraints as similar as possible to the theoretical ones. The results confirmed the theoretical prediction of the effective length factor of the diagonal members which exhibited good hysteretic behaviour with large inelastic deformation capacity under cyclic loading. Dimopoulos *et al.* (2012) proposed formulae for the estimation of lateral displacements at first yielding of plane moment resisting and x-braced steel frames. Lin *et al.* (2012) studied the design basis earthquake performance of self-centering moment-resisting frame and the seismic performance of this structure by using nonlinear pushover analysis method. Hosseinzadeh and Mohebi (2016) found the satisfactory brace geometries that minimize instability of the core section while maximizing energy dissipation capacity. Hoveidae *et al.* (2015) found that short-core all-steel buckling restrained braces sustain large plastic deformations without crossing the low cycle fatigue life borders or instability of the encasing system. Piedrafita *et al.* (2015) proposed a new material constitutive model for predicting the hysteretic response and failure of a new all-steel buckling restrained braces. D’Aniello *et al.* (2015) studied the influence of beam stiffness on seismic response of chevron concentric bracings. Salawdeh and Goggins (2013) developed a robust numerical model for cold-formed steel square and rectangular structural hollow sections for use as axial loaded members in earthquake engineering applications. Zahrai and Jalali (2014) presented an experimental investigation on cyclic performance of two knee braced single spanone-story frame specimens. Hassanien Serror *et al.* (2014) evaluated the values of both damping and ductility reduction factors for steel moment resisting frames with supplemental linear viscous dampers.

The above research shows the steel frame behaviors stably and performs very well under earthquake ground motions. However, the seismic performance of steel frame-bent structure has not been reported. This study focuses on the experimental investigating the performance of steel frame-bent structure under cyclic lateral load. The failure mode, deformability, ductility, energy dissipation capacity, stiffness degradation of steel frame-bent structure was studied.

2. The specimen design and test setup

According to the seismic intensity of degree 8, a 1/10 scale models of three-bay and five-story steel frame bent was designed in accordance with Chinese Code GB50011 (2010) and its details were shown in Fig. 1 and Table 1, in which all the dimensions are in millimeter. The steel frame-bent was made of Q235B steel (China, GB 500172003).The results of the coupon tests for the steel materials used in this test are summarized in Table 2. Fig. 2 showed the partially connections of the structure. And most beam-column connection was welded. There were a few welded-bolted connections in this structure.

The axial load was applied by the hydraulic jacks on the top columns, which is determined by the design axial compression of the real structure. 86 kN force was loaded at the middle column, and no force was loaded at the side column due to the load value was too small, which no effect on the experiment results. Lateral load was applied by a servo controlled hydraulic actuator. During the test process, each story displacement and base slip were measured by eight linear variable displacement transducers (LVDT). In addition, strain gages ware placed on the critical positions of beam flanges and webs, column flanges and webs, connections to measure the strain history during the test process. All data was collected by TDS-602 static data acquisition instrument. The test setup is shown in Fig. 3. And lateral braces were provided at the end of loading beam to prevent its out-of-plane movement.

The cyclic load history was adopted according to a procedure as recommenced in Chinese specification JGJ101-96. Fig. 4 shows the loading procedure of the test specimen. The loading procedure involved two load steps, namely, a load-controlled step and a displacement-controlled step. Load-displacement hybrid control program was applied, in which the lateral loading sequence was controlled by force for the initial loading cycles till the test specimen was observed starting to yield. At the initial loading phase, every load level was applied for one cycle in an increment of 2 kN.When the test specimen started yielding, the loading sequence was controlled by displacement. On the basis of the yield displacement, the target displacements for the cyclic loading were set as the multiple of the yield displacement, the cyclic loadings were repeated three times at each target displacement. When the lateral strength of test specimen dropped to 85% of ultimate strength, the loading was terminated.

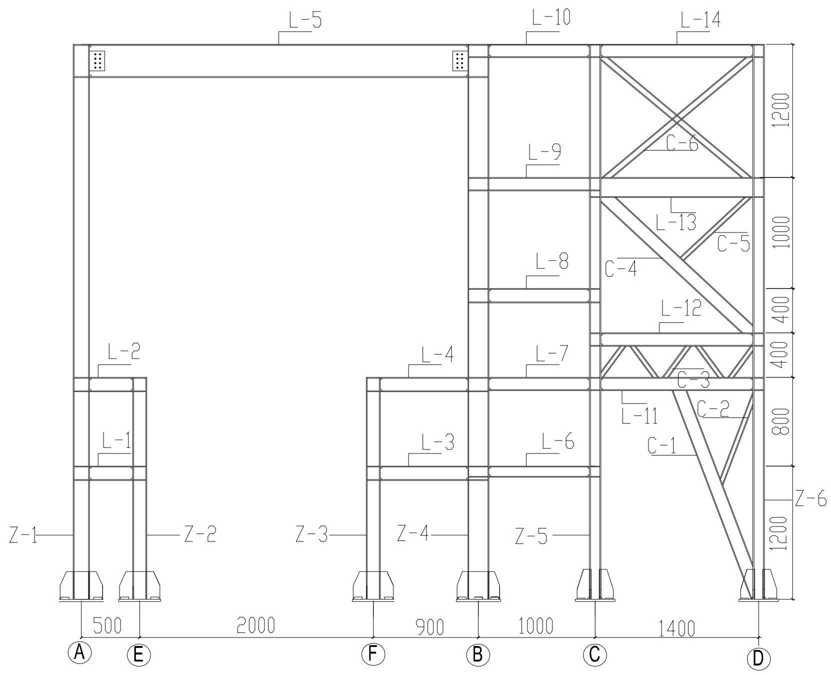

Fig. 1 Dimensions of specimen

(a) (b)

(c) (d)

Fig. 2 Details of connection

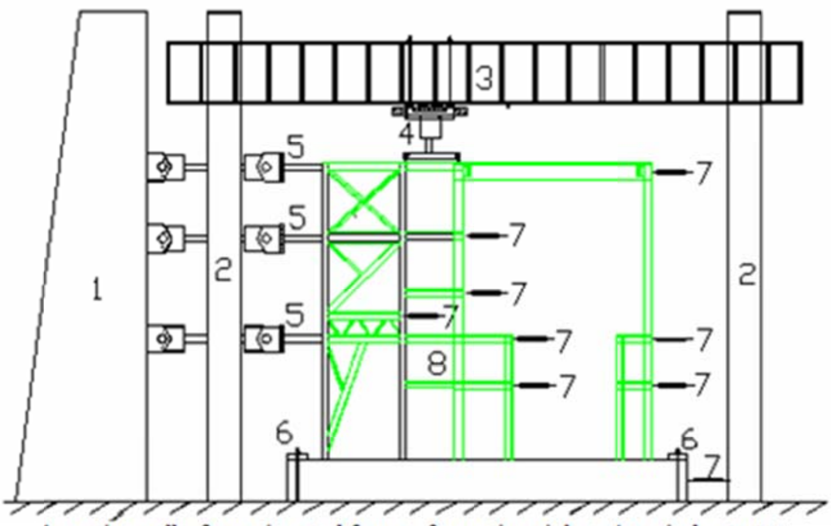

1.reaction wall; 2.reaction steel frame; 3. reaction girder; 4.vertical actuator;
5.horizontal actuator; 6.tie bolt; 7.displacement transducer; 8.test specimen

(a)

Fig. 3 Test setup

(b)

Fig. 3 Continued

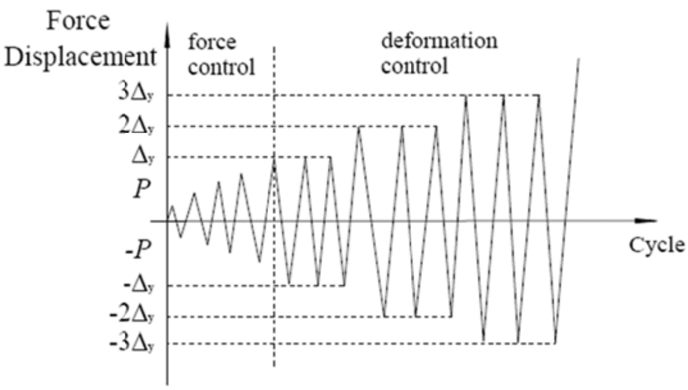

Fig. 4 Loading procedure of the test

Table1 Component dimensions

Member	Number	Dimensions(mm)	Member	Number	Dimensions (mm)
column	Z-1	H140×70×6×8		L-1、L-2、 L-3、L-4、L-8	H 130×50×6×8
	Z-2、Z-3	H 120×60×6×8		L-5	H 300×50×6×8
	Z-4	H 180×90×6×8		L-6	H 100×40×6×8
	Z-5、Z-6	□100×100×10×10 (Box)	beam	L-9	□120×70×6×8 (Box)
brace	C-1、C-4	H 120×60×6×8		L-7、 L-10、L-11、L-12、L-14	H 120×40×6×8
	C-2、C-3、C-5	H 45×30×6×8			
	C-6	H 60×45×6×8		L-13	□180×80×6×8 (Box)

Table 2 Material properties of steel

Thickness(mm)	Yield stress (MPa)	Ultimate stress (MPa)	Modulus of elasticity (GPa)
6	340.6	463.2	194
8	325.6	441.7	208
10	321.8	450.8	195

3. Experimental results

3.1 Failure pattern

During the 120 kN cycle of the middle horizontal actuator, the test specimen appeared to be elastic. During the 40 mm cycle, the weld cracks appeared at the bottom flange of Beam L-6 right end connected to the column (Fig. 5(a)), the top flange of Beam L-6 left end connected to the column, the top flange of Beam L-7 right end connected to the column, the bottom flange of Beam L-7 left end connected to the column, respectively. The web buckling of Beam L-12 was observed. During the 65 mm cycle, the weld cracks appeared at the bottom flange of Beam L-8 right end connected to the column and the top flange of Beam L-8 left end connected to the column. The second brace fractured from left to right at the second story (Fig. 5(b)).The bottom flange of right Beam L-6 and top flange of left Beam L-6 were snapped. The steel brace C-4 buckling was appeared (Fig. 5(c)). During the 80 mm cycle, the weld cracked at the Beam L-10 left end connected to the column, Beam L-11 broken (Fig. 5(d)). During the 90 mm cycle, the third brace fractured from left to right at the second story. During the 100 mm cycle, the fourth brace fractured from left to right at the second story. Beam L-12 broken, and the failure patterns of test specimen was shown in Fig. 5(e).

3.2 Hysteresis loop and skeleton curves

The lateral load- displacement hysteresis loop of the specimen is shown in Fig. 6. The figure shows that the hysteresis loop has the following features:

(1) In the early stage of horizontal loading, the lateral load- displacement relationship was approximately linear, which explained that the structure was in the elastic state. And there was basically no residual deformation.

(2) With the load increasing, the area of the hysteresis loops continued to grow. And there is a large residual deformation, showed that the structure has entered the nonlinear stage.

(3) After the specimen yielded, with the increasing of the lateral displacement, the lateral load of the specimen gradually increased. Hysteresis loop were even more fullness. Due to the influence of the cumulative damage, the bearing capacity and stiffness of the specimens degenerated. After reaching to the peak load, the residual deformation was obvious, and the stiffness and strength of the structure degraded obviously.

(4) The hysteresis loops were in spindle shape, which shape were full and had larger area. It showed that the structure has good seismic performance.

The skeleton curve of the specimen is shown Fig. 7. It shows that the skeleton curve can be divided into 3 stages or elastic stage, elastic-plastic stage and failure stage. In the elastic stage, the stiffness of the specimens basicily remains the same. When the load reached the yield point, the

(a) The bottom flange of Beam L-6

(b) The brace at the second story

(c) The steel brace C-4

(d) The Beam L-11

(e) Test specimen after failure

Fig. 5 Failure modes of test specimen

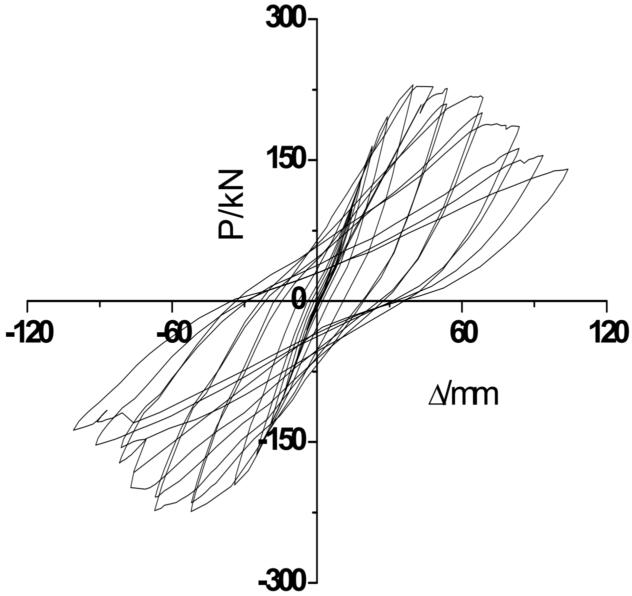

Fig. 6 Hysteretic loops of test specimen

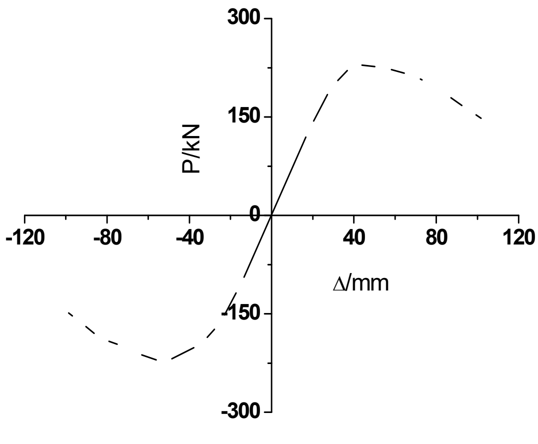

Fig. 7 Skeleton curves of test specimen

beam end and column end yielded, and the stiffness gradually reduced. The skeleton curve of the specimen decreased slowly after the load reached the peak value. It was shown that the test specimen had good late deformability and ductility.

3.3 Inter-story drift ratio

Tables 3, 4 shows the inter-story drift ratio of test specimen. P_y stands for the yield load, which was confirmed with the method of universal yield moment that the process of which is showed in Fig. 8 (Lubliner 2006). P_m stands for the peak load. And P_u stands for the failure load, which corresponding to 85% of the peak load. Δ_y, Δ_p, Δ_f are the displacements correspond to the load P_y, P_m, P_u, respectively. α_y, α_m, α_u are the drift angle correspond to the load P_y, P_m, P_u, respectively. The drift angle is defined as Δ/H, where Δ stands for the top displacement, and H stands for the whole height. δ_y, δ_m, δ_u are the inter-story drift correspond to the load P_y, P_m, P_u, respectively. θ_y, θ_m, θ_u are the inter-story drift ratio correspond to the load P_y, P_m, P_u, respectively.

As shown in Table 3, when the load reached to the failure load, the top displacement and the integrity inter-story drift of the test specimen were 85.7 mm, 1/58, respectively. And the inter-story drift ratio ranged from 1/175 to 1/34.This shown that the structure had excellent deformation capacity.

Table 3 and Table 4 show that the first-story and the second-story were weak layers, which inter-story drift ratio were larger. The inter-story drift ratio in first-story and second-story were 1/39, 1/34, respectively, much larger than the limit value specified by Chinese Seismic Design Code, which was equal to 1/50, shown that the test specimen has a good ability to resist collapse deformation.

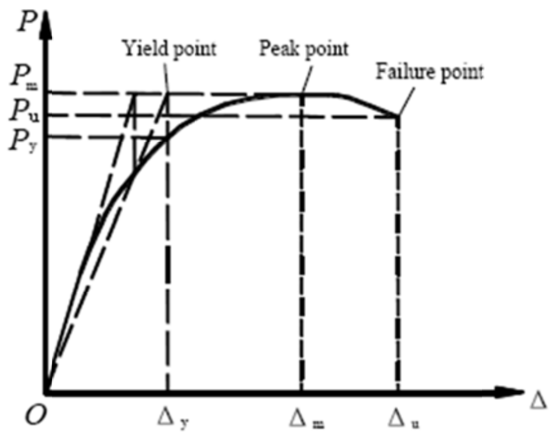

Fig. 8 Method of universal yield moment

Table 3 The inter-story drift ratio of test specimen

Position	Loading direction	Yield point		Peak point		Failure point	
		δ_y/mm	θ_y	δ_m/mm	θ_m	δ_u/mm	θ_u
First-story	Positive	7.1	1/169	14.3	1/84	29.1	1/41
	Negative	8.6	1/139	18.7	1/64	30.1	1/39
Second-story	Positive	4.9	1/163	9.3	1/86	19.0	1/42
	Negative	6.6	1/121	14.7	1/54	23.3	1/34
Third-story	Positive	2.9	1/275	5.2	1/154	11.6	1/68
	Negative	2.0	1/400	7.3	1/110	11.7	1/67
Fourth-story	Positive	2.4	1/416	4.8	1/208	8.6	1/116
	Negative	1.3	1/719	3.5	1/282	5.7	1/175
Fifth-story	Positive	2.9	1/413	6.2	1/195	12.9	1/93
	Negative	2.4	1/500	8.0	1/149	14.9	1/80

Table 4 The experimental results at main loading of test specimen

Position	Loading direction	Yield point			Peak point			Failure point			Ductility coefficient
		P_y/kN	Δ_y/mm	α_y	P_m/kN	Δ_m/mm	α_m	P_u/kN	Δ_u/mm	α_u	μ
Integrity	Positive	144.2	20.2	1/247	230.3	39.7	1/126	195.7	81.2	1/61	4.0
	Negative	131.8	20.9	1/239	224.3	52.2	1/95	190.6	85.7	1/58	4.1

3.4 Displacement ductility coefficient and energy dissipation capacity

Displacement ductility is one of the important indicators reflecting the seismic performance of structures. It is usually represented by displacement ductility coefficient, which was defined as $\mu=\Delta_f/\Delta_y$. From Table 4, it is shown that the integral displacement ductility coefficients positive and negative directions were 4.0 and 4.1, respectively. This is indicated that the ductility of the structure is good and has excellent deformation capacity.

The energy dissipation capacity of the structure, which is an important seismic performance index for structure, is usually evaluated by equivalent viscous damping coefficient h_e. By analyzing the hysteretic loops of the test specimen under low cyclic reversed loading, the degree of energy dissipation under different loading level can be investigated. The equivalent viscous damping coefficient can be written as follows

$$h_e = \frac{1}{2\pi} \cdot \frac{S_{(ABCDA)}}{S_{(OBE+ODF)}} \tag{1}$$

where $S_{(ABCDA)}$ and $S_{(OBE+ODF)}$ represents the area of the hysteretic loops ABCDA and triangles OBE and ODF, respectively, which are showed in Fig. 9. The calculated failure equivalent viscous damping coefficient of the test specimen was 0.191, which approximately equal to equivalent viscous damping coefficient of the steel frame. It indicates that the steel frame-bent structure has a good energy dissipation capacity.

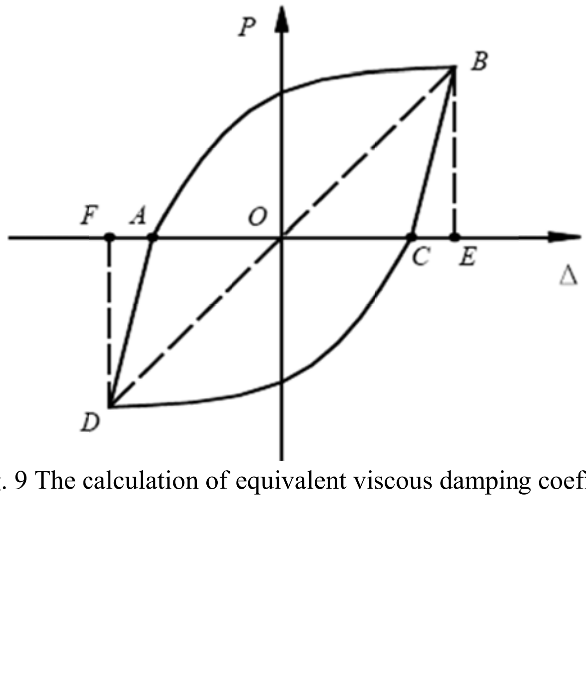

Fig. 9 The calculation of equivalent viscous damping coefficient

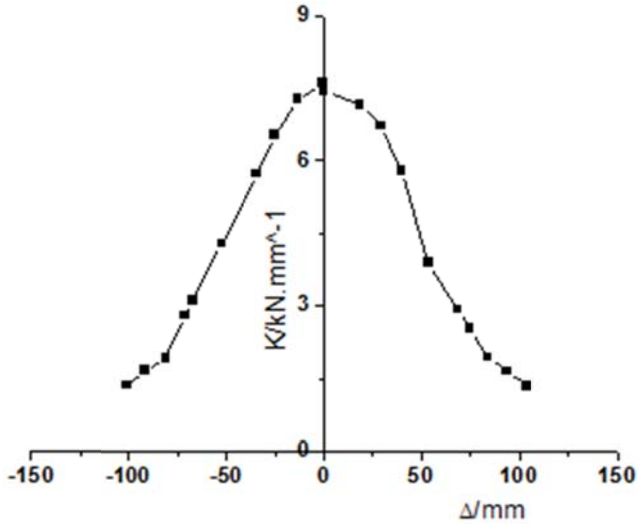

Fig. 10 Curves of stiffness degradation

3.5 Stiffness

Secant stiffness, which used to express the stiffness of the test specimen under low cyclic reversed loading, is the ratio of peak load in every load level and the associated displacements in positive and negative direction. With the top displacement increasing, the stiffness of the specimen degreased gradually, which was defined as stiffness degradation. It reflects the degradation of the resistance of lateral collapse. The stiffness degradation of the test specimen under different loading levels is shown in Fig. 10. It shows that the initial stiffness in positive and negative direction have certain difference. The main reason is that asymmetry of structure, which causes asymmetry of stiffness. With the displacement increasing, the positive and negative stiffness absolute value of specimen is nearly equal. Early the speed of stiffness degradation was fast. After the test specimen yielded, with the development of plastic deformation, the speed of degradation was from fast to slow.

4. Conclusions

The structural behavior of steel frame-bent structure was studied. The specimen with three bay and five stories were tested for cyclic lateral loading. The following conclusions can be drawn from this investigation:

(1) During the loading process, plastic hinges firstly occurred at beam ends, and then occurred at column ends, and the failure mechanism of test specimen was the beam-hinged mechanism.

(2) The hysteresis loops was in spindle shape, which shape was full and had larger area. It showed that the structure had good seismic performance. And the ductility and the energy dissipation capacity were good.

(3) The test specimen had a good ability to resist collapse deformation. The ultimate inter-story drift ratio was 1/34, which was over 1/50. It showed that the test specimen had good deformation

capacity.

(4) With the displacement increasing, the positive and negative stiffness absolute value of specimen is nearly equal. Early the speed of stiffness degradation was fast. After the test specimen yielded, the speed of degradation was from fast to slow.

(5) The multilayer frame is responsible of the energy dissipation of the whole system. And the frame lateral resistance is depended on the mechanical property of the bracing.

Acknowledgments

This work was supported by the Chinese National Natural Science Foundation (No. 51368001), the Natural Science Foundation of Jiangxi Province (20142BAB216002),the Technology Support Project of Jiangxi Province (20151BBG70012) and the Opening Project of Guangxi Key Laboratory of Disaster Prevention and Structural Safety (No. 2013ZDK01), which are gratefully acknowledged.

References

Banihashemi, M.R., Mirzagoltabar, A.R. and Tavakoli, H.R. (2015), "Development of the performance based plastic design for steel moment resistant frame", *Int. J. Steel. Struct.*, **15**(1), 51-62.

Code for design of steel structures(GB50017-2003) (2003), Beijing. (in Chinese)

Code for seismic design of building(GB50011-2010) (2010), Beijing. (in Chinese)

D'Aniello, M., Costanzo, S. and Landolfo, R. (2015), "The influence of beam stiffness on seismic response of chevron concentric bracings", *J. Constr. Steel. Res.*, **112**, 305-324.

Dimopoulos, A.I., Bazeos, N. and Beskos, D.E. (2012), "Seismic yield displacements of plane moment resisting and x-braced steel frames", *Soil. Dyn. Earthq. Eng.*, **41**, 128-140

Grande, E. and Rasulo, A. (2015), "A simple approach for seismic retrofit of low-rise concentric X-braced steel frames", *J. Constr. Steel. Res.*, **107**, 162-172

Grande, E. and Rasulo, A. (2013), "Seismic assessment of concentric X-braced steel frames", *Eng. Struct.*, **49**, 983-995.

Hassanien Serror, M., Adel diab, R. and Ahmed Mourad, S. (2014), "Seismic force reduction factor for steel moment resisting frames with supplemental viscous dampers", *Earthq. Struct.*, **7**(6), 1171-1186.

Hosseinzadeh. Sh. and Mohebi, B. (2016), "Seismic evaluation of all-steel buckling restrained braces using finite element analysis", *J. Constr. Steel. Res.*, **119**, 76-84.

Hoveidae, N., Tremblay, R., Rafezy, B. and Davaran, A. (2015), "Numerical investigation of seismic behavior of short-core all-steel buckling restrained braces", *J. Constr. Steel. Res.*, **114**, 89-99

Hsu, H.L. and Li, Z.C. (2015), "Seismic performance of steel frames with controlled buckling mechanisms in knee braces", *J. Constr. Steel. Res.*, **107**, 50-60.

Kamaris, G.S., Hatzigeorgiou, G.D. and Beskos, D.E. (2015), "Direct damage controlled seismic design of plane steel degrading frames", *Bull. Earthq. Eng.*, **13**(2), 587-612.

Lin, Y.C., Sause, R. and Ricles, J.M. (2013), "Seismic performance of steel self-centering, moment-resisting frame: Hybrid simulations under design basis earthquake", *J. Struct. Eng.*, **139**(11), 1823-1832.

Lubliner, J. (2006), *Plasticity Theory*, Pearson Education, Upper Saddle River, NJ, USA.

Metelli, G. (2013), "Theoretical and experimental study on the cyclic behaviour of X braced steel frames", *Eng. Struct.*, **46**, 763-773.

Ministry of Construction. Specificating of testing methods for earthquake resistant building (JGJ101-96) (1997), Beijing. (in Chinese)

Nguyen, P.C. and Kim, S.E. (2014), "Nonlinear inelastic time-history analysis of three-dimensional semi-

rigid steel frames", *J. Constr. Steel. Res.*, **101**, 192-206.
Piedrafita, D., Maimí, P. and Cahis, X. (2015), "A constitutive model for a novel modular all-steel buckling restrained brace", *Eng. Struct.*, **100**(1), 326-331.
Pollino, M. (2015), "Seismic design for enhanced building performance using rocking steel braced frames", *Eng. Struct.*, **83**(15), 129-139.
Salawdeh, S. and Goggins, J. (2013), "Numerical simulation for steel brace members incorporating a fatigue model", *Eng. Struct.*, **46**, 332-349.
Stamatopoulos, G.N. (2014), "Seismic response of steel frames considering the hysteretic behaviour of the semi-rigid supports", *Int .J. Steel. Struct.*, **14**(3), 609-618.
Tenchini, A., D'Aniello, M., Rebelo, C., Landolfo, R., Silva, L.S. and Lima, L. (2014), "Seismic performance of dual-steel moment resisting frames", *J. Constr. Steel. Res.*, **101**, 437-454.
Zahrai, S.M. and Jalali, M. (2014), "Experimental and analytical investigations on seismic behavior of ductile steel knee braced frames", *Steel Compos. Struct.*, **16**(1), 1-21.

CC